Testing and modelling of multiple-leaf masonry walls under shear and compression

J. Pina-Henriques & P.B. Lourenço
University of Minho, Department of Civil Engineering, Guimarães, Portugal
L. Binda & A. Anzani
Politecnico di Milano, Department of Structural Engineering, Milano, Italy

ABSTRACT: Predicting the behaviour of multiple-leaf masonry walls is a challenging issue, given the influence of a wide range of factors as the mechanical properties of the leaves, their dimensions and the way they are connected to each other. In the present paper, experimental results in large specimens are carefully reviewed together with numerical interpretation of the shear and compressive behaviour of multiple-leaf walls. Simplified calculations for practical assessment of existing walls are also addressed.

1 INTRODUCTION

Multiple-leaf walls are frequently found in ancient buildings. They usually consist of two or three leaves made up of different materials such as stone, brick or rubble masonry. For an appropriate repairing/strengthening of masonry walls with minimum intervention, the bearing capacity of the structure has to be known prior to the intervention. However, this task is especially complex in the case of multiple-leaf walls, because the stress distribution is largely dependent on the mechanical properties of the leaves, on their dimensions and on the way they are connected to each other. In particular, the load transfer between leaves is a key issue when studying compressive damage of heavy pillars in monumental buildings, see Binda *et al.* (2003a).

References in literature can be found on this topic, see e.g. Binda *et al.* (1991), Egermann & Neuwald-Burg (1994), Binda *et al.* (1994) and Drei & Fontana (2001). Yet, further experimental and numerical insight on the shear and compressive behaviour of composite walls is needed. For this purpose, a set of twelve three-leaf stone wallets (regular-rubble-regular) with dimensions of 310 × 510 × 790 mm^3 were built and tested at the Politecnico di Milano, within the frame of a National Research Contract (resp. L. Binda), see Binda *et al.* (2003b). Two types of collar joints (with and without shear keys) and two types of stones (a limestone named Noto and a sandstone named Serena) have been considered. The wallets were tested according to three different procedures:

a) Shear tests. A monotonic load was applied to the inner-leaf while the outer-leaves were supported. This test is similar to the EN 1052-3 (CEN, 2002).
b) Compression tests on single leaves. Outer and inner leaves were tested individually under uniaxial compression.
c) Compression tests on full wallets. A monotonic load was applied to the complete transversal section of the wallets.

This paper addresses the results obtained in the experimental tests and their critical analysis, resorting to simplified calculations and, also, to sophisticated numerical tools.

2 EXPERIMENTAL TESTS

Tests were carried out on the wallets given in Table 1. The specimens dimensions are shown in Figure 1. The same type of stone was used both for the outer and inner leaves.

Table 1. Designation of the wallets according to the type of stone and connection.

	Straight collar joints	Keyed collar joints
Noto limestone	NS1, NS2, NS3	NO1, NO2, NO3
Serena sandstone	SS1, SS2, SS3	SO1, SO2, SO3

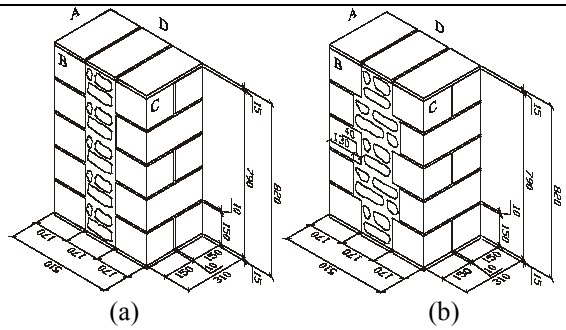

(a) (b)

Figure 1. Wallets dimensions in *mm*: (a) straight collar joints and (b) keyed collar joints.

2.1 *Characterization of masonry components*

Physical and mechanical tests were carried out on cylindrical samples cored from the stone units used to build the wallets. The units were cored considering two different orientations: along the loading direction L and along the bedding direction B, so that the anisotropy of the material could be characterized.

The physical tests consisted on the determination of the bulk density and open porosity, according to EN 772-4 (CEN, 1998). Six cylindrical specimens with a diameter of 80 *mm* and a height of 145 *mm* were considered for each type of stone. The average results obtained in terms of the bulk density $\rho_{b,s}$ and the open porosity P_o are given in Table 2. In addition, the coefficient of variation CV is also given. The values found illustrate the significantly different physical properties of the two stones. The Noto limestone exhibits high open porosity and low weight while the Serena sandstone exhibits a 1.5 times larger weight and seven times less porosity.

Table 2. Average results of the bulk density and open porosity of the stones.

Type of stone	$\rho_{b,s}$ kg/m^3	*C.V.* %	P_o %	*C.V.* %
Noto	1760	1.5	15.4	4.5
Serena	2570	0.3	2.1	5.7

Uniaxial compressive tests were carried out after the physical tests, on the same cylindrical samples, according to EN 772-1 (CEN, 2000). Three specimens for each combination type of stone/orientation were tested. The average values for the compressive strength f_c, the peak strain ε_p, the modulus of elasticity E and the coefficient of Possion ν are given in Table 3. According to the results obtained, the Serena stone exhibits, in the loading direction, a strength about five times larger than the Noto stone and about the double of the stiffness.

Table 3. Average results obtained from the compression tests on the stones (values in brackets give the *CV*).

Type of stone	Orientation	f_c N/mm^2	ε_p 10^{-3}	E N/mm^2	ν -
Noto	L	20.6 (7%)	2.4	9475	0.10
Noto	B	17.6 (22%)	2.3	8525	0.09
Serena	L	104.2 (1%)	*	18218	0.19
Serena	B	89.0 (15%)	*	23293	0.21

* The Serena specimens had to be tested in a machine with a higher capacity, which did not allow recording the displacement values.

The tensile strength was obtained resorting to the indirect tension test (splitting test), according to the RILEM recommendation CPC6, RILEM (1994). The tests were carried out on six cylindrical specimens for each type of stone with a diameter and height of 80 *mm*. The specimens were cored along the bedding direction of the units. This direction is the most relevant with respect to the tensile strength as it is the direction where the principal tensile stresses occur when units are vertically loaded.

The average results obtained are given in Table 4. In the case of concrete, the splitting tensile strength $f_{t,s}$ is about 5 to 12% higher than the direct tensile strength f_t, see Neville (1997). Here, f_t has been considered equal to $0.9\,f_{t,s}$. According to the results obtained, the Noto stone exhibits an average tensile strength three times smaller than the Serena stone. Relatively to the ratio between the compressive and tensile strengths, a value of ten times was found for the Noto stone and a value of seventeen times was found for the Serena stone.

Table 4. Average results obtained from the tension tests on the stones (values in brackets give the *CV*).

Type of stone	Orientation	$f_{t,s}$ N/mm^2	f_t N/mm^2
Noto	B	2.05 (13%)	1.8
Serena	B	6.00 (12%)	5.4

A commercial premixed hydraulic lime mortar denominated *Albaria Allettamento*, Italy, was adopted to build the wallets. Flexural and compressive tests have been carried out according to EN 1015-11, (CEN, 1999). The tests were performed at four ages: 28 days, 75 days (corresponding to the beginning of the tests), 90 days and 172 days (corresponding to the end of the testing programme). For each curing stage a total of six prisms were tested.

Table 5 gives the average results obtained for the flexural strength f_f and for the compressive strength f_c. The results found yield average values for the flexural and compressive strengths during the testing period (75 to 172 days) of 2.2 N/mm^2 and 10.3 N/mm^2. Generally, a factor of 1.5 can be assumed for the ratio between flexural and tensile strengths, see Van der Pluijm (1999) and Lourenço (1997).

Table 5. Average results obtained from the flexural and compression tests on the mortar (values in brackets give the *CV*).

Curing time *Days*	f_f N/mm^2	f_c N/mm^2
28	1.5 (6%)	7.4 (3%)
75	1.9 (13%)	9.2 (6%)
90	2.3 (10%)	9.7 (7%)
172	2.2 (9%)	11.2 (5%)

2.2 *Results of shear tests*

Two wallets for each combination type of stone – type of connection were tested in a total of eight specimens, see also Binda *et al.* (2003c) and Anzani *et al.* (2003).

The load-displacement diagrams obtained are illustrated in Figure 2. In the case of the wallets with straight collar joints, a non-symmetric response of the connections was found, with failure occurring non-simultaneously. Such behaviour had also been found by Lourenço *et al.* (2004) in triplet tests per-

formed on three courses brick masonry panels and must be considered characteristic of the triplet test.

The first peak in the diagrams of Figure 2a corresponds to the failure of the weakest connection and provides the shear strength τ_r for a shear area of $2 \times 310 \times 790\ mm^2$. After failure of the first connection a minor rotation of the two leaves still connected was observed due to the eccentricity of the applied load. From that point on the test cannot be intended as a triplet test due to the change in the loading scheme and, therefore, the values related to the second connection to fail should be considered carefully. Namely, the second peak represents the combination of a higher shear strength for the second joint and some minor friction in the first joint due to bending. If the effect of bending is neglected the second peak provides the shear strength of the strongest joint τ_r', for a shear area of $310 \times 790\ mm^2$. This holds true only because no confining pressure is present.

For the wallets with keyed collar joints, the shear strength was calculated assuming straight connections and, thus, the value represents an "equivalent" shear strength.

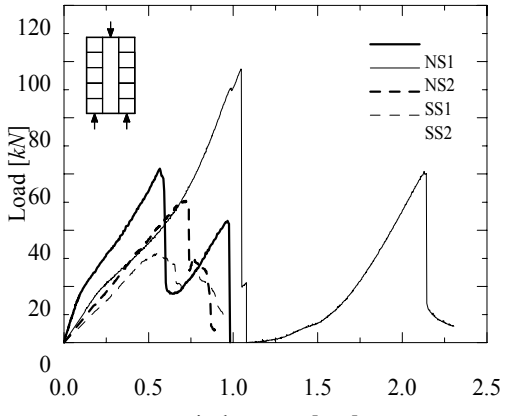

(a)

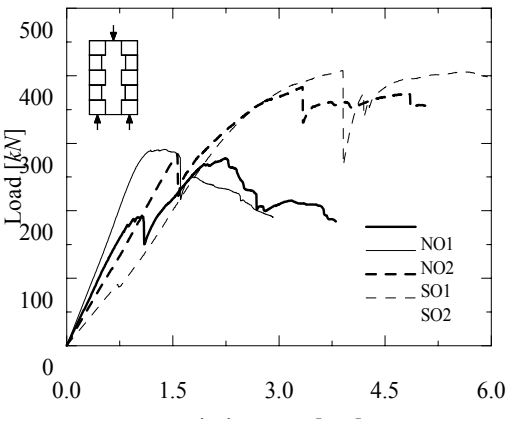

(b)

Figure 2. Load-displacement diagrams obtained for the shear tests: (a) straight collar joints and (b) keyed collar joints.

Table 6 gives, in the case of straight collar joints wallets, the average shear strengths (τ_r and τ_r') and displacements (δ and δ') corresponding to the first and second load peaks. For keyed collar joints wallets, the average values of the shear strength and the corresponding displacements are given.

Table 6. Average results obtained from the shear tests.

Wallets	Type of stone	Type of connection	τ_r N/mm^2	δ mm	τ_r' N/mm^2	δ' mm
NS1,NS2	Noto	Straight	0.17	0.81	0.22	1.55
SS1,SS2	Serena	Straight	0.09	0.64	0.11	0.78
NO1,NO2	Noto	Keyed	0.58	1.82	-	-
SO1,SO2	Serena	Keyed	0.81	3.62	-	-

It is possible to verify that the shear strength of the straight collar joints wallets is mainly influenced by the physical properties of the stone (larger porosity yields better adhesion stone-mortar) while for the keyed collar joints wallets, the strength of the stone is an issue that must be considered.

In terms of ductility the specimens with straight collar joints show a similar behaviour for both types of stones. The failure is quite brittle and without showing any residual strength, given that the test set-up allows the wallets to move freely outwards. Regarding the wallets with keyed collar joints, the Serena specimens exhibit a less brittle behaviour than the Noto specimens. This is probably due to the different behaviour found for the inner-leaves as it will be shown bellow.

Typical ultimate crack patterns are illustrated in Figure 3. The wallets with straight collar joints failed due to the development of two vertical shear cracks along the connections. No other visible damage was observed at the end of the test.

In the case of the specimens with keyed collar joints, the cracking pattern was different according to the type of stone. For the Noto specimens, damage was observed in both outer and inner leaves. In the inner-leaves, more severely damaged, diagonal cracks were observed, developing from the shear keys and passing through the inner-leaf stones. Relatively to the outer-leaves, diagonal cracks near the base appeared. At ultimate stage, full separation in three irregular leaves could be observed.

In the Serena specimens, the cracks developed only in the inner-leaf. However, in this case, cracks usually went around the stones instead of breaking them, due to the larger strength and smaller adhesion stone-mortar. At ultimate stage, it is clearer to observe that only the inner-leaf collapsed.

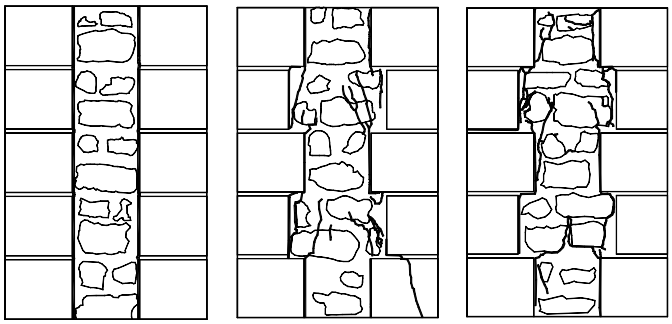

(a) (b) (c)

Figure 3. Typical ultimate crack patterns for (a) straight collar joints wallets (NS1) and keyed collar joints wallets: (b) Noto (NO1) and (c) Serena (SO2).

2.3 *Results of compression tests on single leaves*

The tests were performed on the leaves of the wallets with straight collar joints, previously tested in shear, see Section 2.2 and Binda *et al.* (2003c). In the case of the Noto specimens, both outer-leaves were tested simultaneously, trying to reproduce what may happen in real composite walls: shear failure of the connections followed by transfer of almost all the load to the external stiffer elements. This can explain the type of damage found in massive pillars, see Binda *et al.* (2003a) In the case of the Serena leaves, which were much more resistant, the same procedure could not be adopted due to the limited capacity of the testing machine and, thus, the leaves had to be tested separately.

A comparison between the stress-strain diagrams obtained for the outer and inner leaves is shown in Figure 4. The average results obtained, including the strength f_c, the peak strain ε_p, the elastic modulus E and the Poisson coefficient ν are given in Table 7.

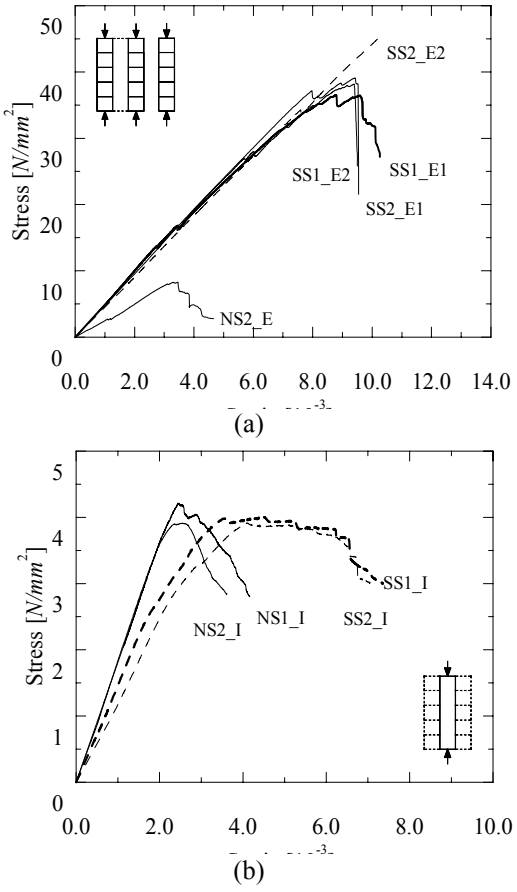

Figure 4. Stress-strain diagrams obtained: (a) outer-leaves and (b) inner-leaves. A problem in the acquisition system prevented fully capturing the NS1_E diagram and, thus, it is not shown. It is also noted that failure of specimen SS2_E2 could not be attained within the capacity of the testing machine.

Table 7. Average results obtained.

Specimen	Stone type	Leaf	P. load *kN*	f_c *N/mm²*	ε_p 10^{-3}	E *N/mm²*	ν -
NS_E	Noto	outer	912	8.7	3.3	3150	-
SS_E	Serena	outer	2095	39.8	9.5	4870	-
NS_I	Noto	inner	214	4.1	2.6	1830	0.15
SS_I	Serena	inner	209	4.0	4.3	1405	0.18

From the given results it is possible to verify that the Noto outer-leaves exhibit a strength of about 45% the stone strength and the inner-leaf about 20%. In the case of the Serena leaves, the same ratios are about 40% for the outer-leaves and only 4% for the inner-leaf. It is further noted that Serena inner-leaves exhibit a less brittle behaviour than Noto specimens, due to the higher strength of the stones, forcing cracks to go around them instead of passing through.

Typical ultimate cracks patterns are illustrated in Figure 5 and Figure 6 for the outer and for the inner leaves, respectively. The shaded areas indicate spalling of the stone.

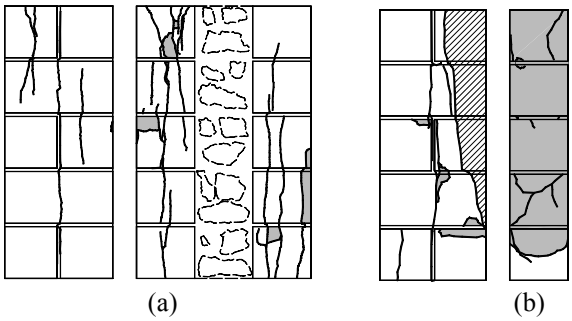

Figure 5. Typical ultimate failure patterns for the outer-leaves: (a) Noto stone and (b) Serena stone.

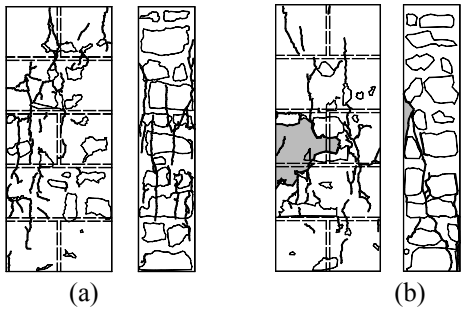

Figure 6. Typical ultimate failure patterns for the inner-leaves: (a) Noto stone and (b) Serena stone.

2.4 *Results of compression tests on full wallets*

One wallet of each type (stone/connection combination) was tested in compression, in a total of four specimens. Yet, the peak load for the Serena wallets was beyond the capacity of the testing machine and a maximum load of 2380 kN was applied. The stress-strain diagrams obtained are shown in Figure 7. Table 8 gives the results found.

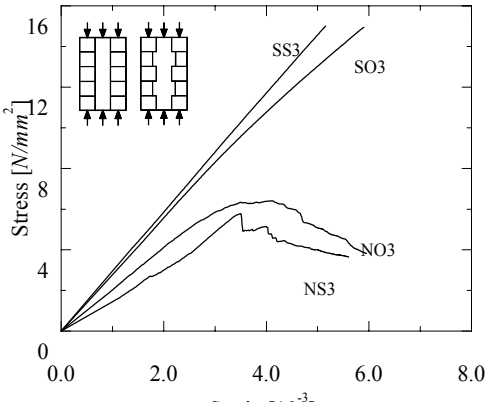

Figure 7. Stress-strain diagrams obtained.

Table 8. Results obtained for the compression tests.

Wallet	Type of stone	Type of connection	Peak load *kN*	f_c N/mm^2	ε_p 10^{-3}	E N/mm^2
NS3	Noto	straight	913	5.8	3.5	1770
SS3	Serena	straight	> 2380	> 15.1	> 5.2	2940
NO3	Noto	keyed	1013	6.4	4.1	2085
SO3	Serena	keyed	> 2380	> 15.1	> 5.9	2725

The following observations can be made from the results, even if the limited number of tests precludes any conclusive statement:

- The strength of the Noto wallet with keyed joints seems to be about 10% higher than the wallet with straight collar joints.
- The Noto wallet with keyed collar joints seems to exhibit a less brittle behaviour than the wallet with straight collar joints.
- The peak load of any of the two Noto wallets tested is not much higher than the peak load of the single outer-leaves: 912.3 *kN*.

The ultimate failure patterns are illustrated in Figures 8 and 9. The shaded areas indicate spalling of the stone. The Noto wallet with straight connections failed due to the development of several vertical cracks in the outer-leaves while the inner-leaf was practically undamaged.

In the case of the Noto wallet with keyed connections the outer-leaves exhibited a more severe and diffuse cracking pattern with several vertical cracks developing in the inner-leaf near the peak load. Regarding the Serena wallet with keyed connections and despite the fact that the peak load was not attained, the development of some cracks in the inner-leaf could be observed.

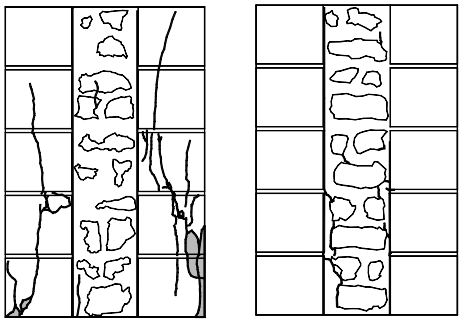

(a) (b)

Figure 8. Ultimate failure patterns for the wallets with straight collar joints: (a) Noto (NS3) and (b) Serena (SS3).

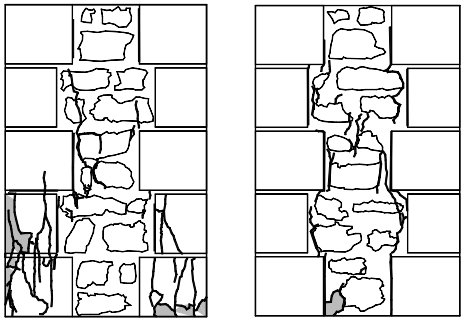

(a) (b)

Figure 9. Ultimate failure patterns for the wallets with keyed collar joints: (a) Noto (NO3) and (b) Serena (SO3).

3 PRELIMINARY SIMPLIFIED CALCULATIONS

This section contains a first analytical interpretation of the test results, with simple calculations being used to predict the compressive strength of the wallets tested. It is noted that the experimental results found should be considered as indicative and conclusions should be taken carefully due to the small number of specimens.

The compressive strength of composite sections f_c can be estimated resorting to the following equations, each one assuming different hypotheses:

(a) the external load is completely supported by the stiffer elements, i.e., the outer-leaves

$$f_c = \frac{2\,t_e}{2\,t_e + t_i} \cdot f_e \tag{1}$$

(b) the external load is supported by each leaf according to its cross-sectional area ratio

$$f_c = \frac{2\,t_e}{2\,t_e + t_i} \cdot f_e + \frac{t_i}{2\,t_e + t_i} \cdot f_i \tag{2}$$

(c) the external load is supported by each leaf according to its area ratio and adjusted by a correction factor, see Egermann and Neuwald-Burg (1994)

$$f_c = \frac{2\,t_e}{2\,t_e + t_i} \cdot \theta_e \cdot f_e + \frac{t_i}{2\,t_e + t_i} \cdot \theta_i \cdot f_i \tag{3}$$

In the above, t_e and t_i are the thicknesses of the outer and inner leaves and f_e and f_i are the uniaxial compressive strengths of the outer and inner leaves. The parameters θ_e and θ_i are correction factors for the outer and inner leaves, assuming that the outer-leaves are under biaxial compressive stresses and bending moments and, thus, their uniaxial strength should be reduced and that the inner-leaf is under a biaxial compressive state of stress and, therefore, its uniaxial strength should be increased.

The results obtained for the wallets with and without shear keys are given in Table 9. In the case of the wallets with keyed collar joints, the thickness assumed for the inner-leaf includes the length of the shear keys. With respect to the application of Eq. (3), the values adopted for the correction parameters were $\theta_e = 0.7$ and $\theta_i = 1.3$, see Egermann and Neuwald-Burg (1994). It is further noted that Eq. (1) was not used to estimate the strength of the wallets with keyed joints because, in this case, it is clear that the inner-leaf is collaborating in the composite response.

Table 9. Predicted compressive strength values for the tested wallets.

Wallet	Type of stone	Type of connection	Exp. f_c N/mm^2	Predicted f_c $[N/mm^2]$ Eq. (1)	Eq. (2)	Eq. (3)
NS3	Noto	straight	5.8	5.8	7.2	5.8
SS3	Serena	straight	> 15.1	25.3	26.6	19.4
NO3	Noto	keyed	6.4	-	6.4	5.7
SO3	Serena	keyed	> 15.1	-	21.3	16.1

The value predicted for the compressive strength of the wallets with straight collar joints using Eq. (1) and Eq. (3) show an excellent agreement with the experimental results. Note that, however, the fact that the experimental and the predicted values are exactly the same should be considered just as a coincidence. The stress-strain diagrams illustrated in Figure 10a show that the inner-leaf vertical deformation do not accompany the vertical deformations of the outer-leaves and that, at failure, the inner-leaf strain is quite less than its peak strain, see also Figure 11a. As a consequence, the bearing capacity of the inner-leaf is only partially mobilized and the hypothesis of Eq. (1) holds fairly true. The causes for the different deformations in the wallet leaves are not completely clear but a possible reason may be attributed to settling of the inner-leaf prior to testing.

In the case of the wallets with keyed collar joints, Eq. (2) yielded the best result while the strength predicted by Eq. (3) is less than the experimental value for the Noto wallets. This indicates that the inner-leaf is collaborating in the wallets response, as confirmed by Figures 10b and 11b, but the assumptions of a strength reduction of the outer-leaves due to bending and a strength increase of the inner-leaf due to confinement do not apply. This can be explained by the test boundary conditions, which allow horizontal displacements at the top and bottom of the wallets. In such way, the effects of outer-leaves bending and inner-leaf confinement are diminished.

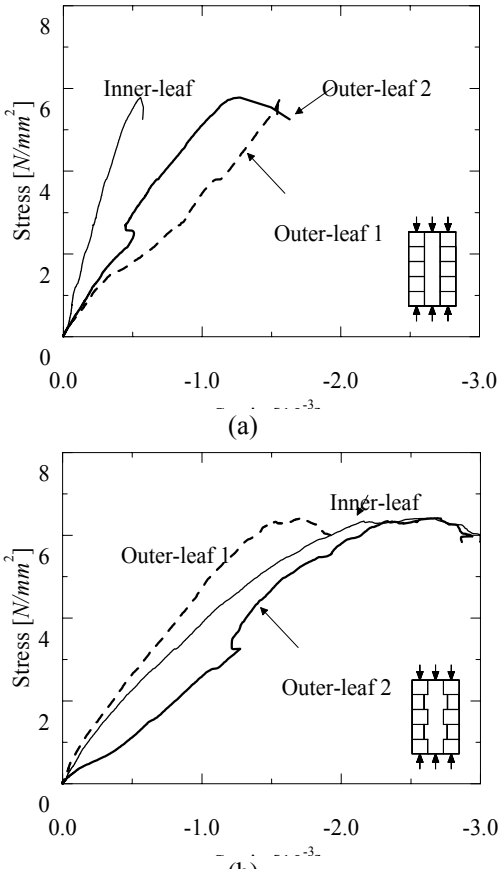

Figure 10. Compression stress-strain diagrams of the leaves inside the composite Noto wallets: (a) straight collar joints (NS3) and (b) keyed collar joints (NO3).

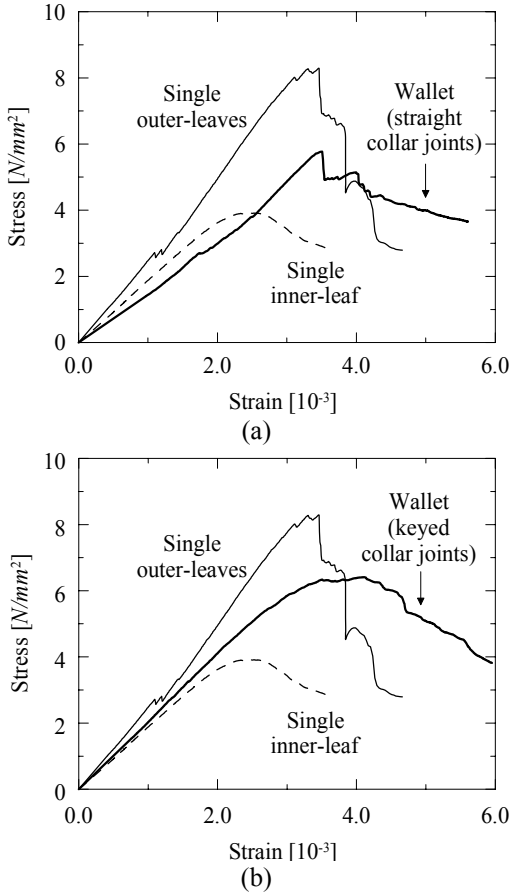

Figure 11. Compression stress-strain diagrams of the single Noto inner and outer leaves and of the full wallets with: (a) straight collar joints (NS3) and (b) keyed collar joints (NO3).

Finally, it should be noted that each equation considered independently predicts a larger strength for the wallets with straight collar joints than for the wallets with keyed collar joints. This is due to the reduction of the cross-sectional area of the outer-leaves in the case of the specimens with shear keys. However, the opposite behaviour was found in experiments. The reason of such behaviour can be attributed to the fact, as already mentioned, that the inner-leaf was almost not collaborating in the experimental response, in the case of wallets with straight collar joints.

4 NUMERICAL SIMULATIONS

This chapter deals with the numerical simulation of the tests performed and represents a relevant contribution towards the interpretation of the results. The leaves of the wallets were represented using plane stress continuum elements (8-noded) with 2×2 Gauss integration while line interface elements (6-noded) with 3×3 Lobatto integration have been adopted for the collar joints. The analyses were carried out with indirect displacement control with line searches. It is further noted that the self-weight of the wallets was not considered.

For the material behaviour, a composite plasticity model with a Drucker-Prager yield criterion in compression and a Rankine yield criterion in tension was

adopted. The inelastic behaviour exhibits a parabolic hardening/softening diagram in compression and an exponential-type diagram in tension. The material behaves elastically up to one-third of the compressive strength and up to the tensile strength. For the interface elements a combined cracking-shearing-crushing model developed by Lourenço (1996a) was adopted. The compressive mode was, however, not active and interface failure could only occur by shear or/and tensile yielding. Both shear and tensile modes exhibit exponential-type softening.

The elastic material properties adopted for the wallets leaves are given in Table 10 and the inelastic properties in Table 11. Here, E is the elastic modulus, ν is the Poisson coefficient, c is the cohesion, f_t is the tensile strength, ϕ is the friction angle, ψ is the dilatancy angle, Gf_c is the compressive fracture energy and Gf_I is the tensile fracture energy. The cohesion is obtained from Eq. (4), which derives from the Drucker-Prager yield function applied to uniaxial compression. Here, f_c is the compressive strength. The tensile strength of the outer-leaves was considered equal to the tensile strength of the stone, assuming, thus, vertical cracking. The tensile strength of the inner-leaf was obtained according to $f_t = f_c/15$, which is a relation often found for masonry specimens. The value adopted for the friction angle was 10º (a larger value in plain stress would implicate an overestimation of the biaxial strength) and, for the dilatancy angle, a value of 5º was assumed. For the tensile fracture energy, a value in agreement with the experimental results reported by Van der Pluijm (1999) for brick specimens was adopted. Values of the elastic modulus and of the compressive fracture energy were adopted so that the numerical response of the specimens resembled the experimental response, see Figure 12.

$$c = \frac{1-\sin\phi}{2\cos\phi} f_c \tag{4}$$

Table 10. Elastic properties for the wallets leaves.

Material	E N/mm^2	ν -
Outer-leaves	3150	0.10
Inner-leaf	2100	0.15

Table 11. Inelastic properties for the wallets leaves.

Material	c N/mm^2	f_t N/mm^2	$\sin\phi$ -	$\sin\psi$ -	Gf_c N/mm	Gf_I* N/mm
Outer-leaves	3.7	1.8	0.17	0.09	5.0	0.070
Inner-leaf	1.7	0.3	0.17	0.09	5.0	0.035

* For the shear simulations of the keyed wallets, the values adopted for Gf_I were 0.150 (outer-leaves) and 0.070 *N/mm* (inner-leaf), so that numerical convergence could be found.

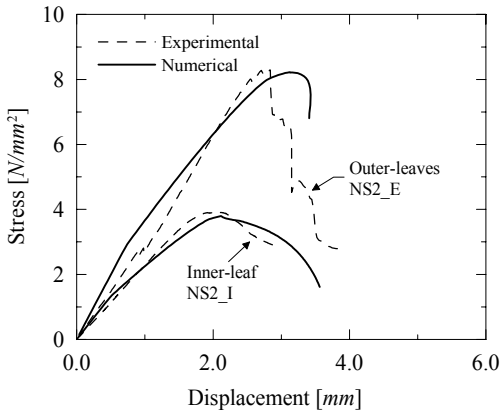

Figure 12. Stress-displacement diagrams for the leaves of the Noto wallets.

The elastic material properties assumed for the collar joints are given in Table 12 and the inelastic properties are given in Table 13. The parameters were obtained, whenever possible, from the shear test on wallet NS1 but most of the inelastic parameters are unknown and must be estimated. The interfaces shear stiffness k_s was adopted so that the numerical and experimental elastic responses showed a good agreement. Based on elastic assumptions, the normal stiffness k_n can be obtained according to $k_n = k_s \times 2(1+\nu) = 1.0\ N/mm^3$, where $\nu = 0.2$ is the coefficient of Poisson. However, higher values had to be adopted in order to avoid interpenetration of the two continuums separated by the interfaces. The cohesion c for the first connection to fail was given experimentally but for the second connection a value was adopted so that the numerical response resembles the experimental response. The values of the remaining inelastic parameters (tensile strength f_t, friction coefficient $\tan\phi$, dilatancy coefficient $\tan\psi$, mode I fracture energy Gf_I and mode II fracture energy Gf_{II}) were adopted in agreement with the values experimentally found by Van der Pluijm (1999) and recommended by Lourenço (1996b) for unit-mortar interfaces.

Table 12. Elastic properties for the collar joints.

Collar joint	k_n * N/mm^3	k_s N/mm^3
1 (left)	150	0.4
2 (right)	150	0.4

* For the shear tests on straight collar joints wallets a lower value of 10 N/mm^3 was adopted.

Table 13. Inelastic properties for the collar joints.

Collar joint	c N/mm^2	f_t N/mm^2	$\tan\phi$ -	$\tan\psi$ -	Gf_I N/mm	Gf_{II} N/mm
1 (left)	0.13	0.09	0.70	0.00	0.015	0.050
2 (right)	0.21	0.14	0.70	0.00	0.015	0.060

4.1 *Shear simulations*

The shear tests for both types of wallets, either with or without shear keys, have been numerically reproduced. As it will become clear later in the text, the testing boundary conditions are a key issue for

the correct interpretation of the results. The experimental test set-up was composed by two steel plates at the bottom, supporting the outer-leaves, and a third plate over the inner-leaf, through which a vertical load was applied. Additionally, sheets of Teflon were placed between the steel plates and the wallets. Therefore, the shear interaction between the plates and the wallets is not a clear issue and must be further investigated.

For the wallets with straight collar joints, this aspect has been assessed by considering four different shear stiffnesses k_s at the supports:

(a) $k_s = 0$, the specimen is free to slide over the steel plates.

(b) $k_s = \infty$, shear slip is precluded between the specimen and the plates.

(c) Intermediate $k_s = 0.01$ N/mm^3, a constant shear stiffness is applied and, thus, shear slip can occur but the horizontal reactions at the boundaries increase with increasing displacement.

(d) Non-linear k_s. At the level of the upper plate, shear slip is free to occur up to a certain relative displacement, beyond which, shear slip is completely restrained. A transition phase for k_s was also considered. At the level of the bottom supports, shear slip is precluded.

Regarding the normal stiffness k_n given to the boundaries, the same behaviour was adopted for all cases. Zero stiffness in tension and infinite stiffness in compression were considered.

Figure 13 illustrates the experimental load-displacement diagram obtained for the wallet NS1 and the numerical diagrams obtained according to the different boundary conditions. It is noted that the two experimental load peaks correspond to the failure of each connection, see Section 2.2.

Regarding the numerical diagrams, some relevant remarks are now given. For boundaries with $k_s = 0$, after failure of the first connection the specimen starts sliding until complete degradation of strength is obtained and, thus, only one of the two connections fails. Another interesting point is that the collapse load is underestimated. Such difference is due to the absence of horizontal constraints at the bottom, which leads to a failure that is not exclusively governed by shear but is accompanied by flexural tensile stresses.

For supports with $k_s = \infty$, a smooth load drop due to material softening follows the failure of the first connection. Yet, it is not as sudden or as deep as the experimental load drop. In terms of collapse loads, the first load peak shows a good agreement with the experimental results but the second load peak, corresponding to the failure of the second connection, is largely overestimated. This is, again, due to the softening behaviour of the first connection to fail, which is still contributing to the specimen strength when the second connection fails.

For an intermediate shear stiffness $k_s = 0.01$ N/mm^3, the value of the first load peak equals the value for $k_s = 0$ and, thus, is also underestimated. After the failure of the first connection, the specimen starts sliding over the boundaries with the load suddenly dropping. However, in this case, after some amount of shear slip, the horizontal reactions at the supports become mobilized and a load increase is observed until failure of the second connection occurs. The comparison with the experimental response shows, nevertheless, that an understiff response was obtained for the second increasing branch.

These results demonstrate that to capture correctly the experimental behaviour found, the boundary conditions adopted must allow some amount of shear slip at the supports after the failure of the first connection and, afterwards, restrain it completely. Therefore, a non-linear k_s was adopted for the upper boundary together with complete shear slip restriction at the bottom boundaries. Good agreement with the experimental response was found, see Figure 13b. Even so, the slope of the second increasing branch is slightly underestimated. This shows that the hypothesis assumed of equal shear stiffness for the two connections is, probably, not true for this specimen, with the second connection showing a stiffer behaviour than the first connection. Figure 14 depicts the progressive shear failure of the wallet.

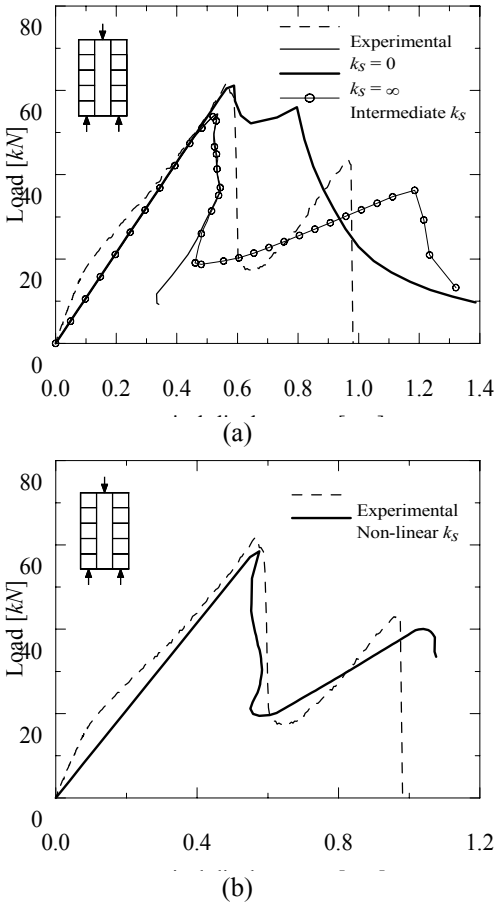

Figure 13. Numerical and experimental (NS1) load-displacement diagrams for straight collar joints wallets. Different shear stiffnesses were considered at boundaries: (a) constant, (b) non-linear.

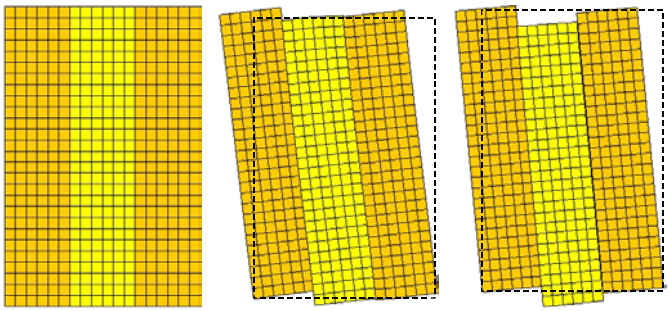

(a) (b) (c)

Figure 14. Progressive shear failure for non-linear k_s boundary conditions: (a) mesh adopted, (b) deformed (incremental) mesh after failure of the first connection and (c) deformed (total) mesh after failure of the second connection.

In the case of keyed collar joints wallets, the influence of the boundary conditions in the response was assessed by a procedure similar to the one utilized for straight collar joints wallets. Here, three different shear stiffnesses at the boundaries were considered: (a) $k_s = 0$, (b) $k_s = \infty$ and (c) intermediate $k_s = 2.0\ N/mm^3$.

The comparison between numerical and experimental load-displacement diagrams is given in Figure 15. The deformed meshes at failure for each numerical diagram are depicted in Figure 16. The collapse load obtained for zero shear stiffness at the boundaries is significantly lower than the experimental collapse load. In this situation, the specimen fails due to a vertical crack that arises in the weaker connection (left), developing along the shear keys. For infinite shear stiffness at the boundaries, a much better agreement with the experimental collapse load is found. Here, failure is governed by crushing of the inner-leaf near the top.

In experimental failure, both described modes seem to be present and, thus, an intermediate k_s was considered in order to reproduce more accurately the behaviour found. The collapse load obtained was almost the same as for $k_s = \infty$ and is about 80% of the experimental collapse load. In this case, failure occurs due to combined shearing-crushing of the inner-leaf near the top and due to the development of vertical cracks along the shear keys, see Figure 16c.

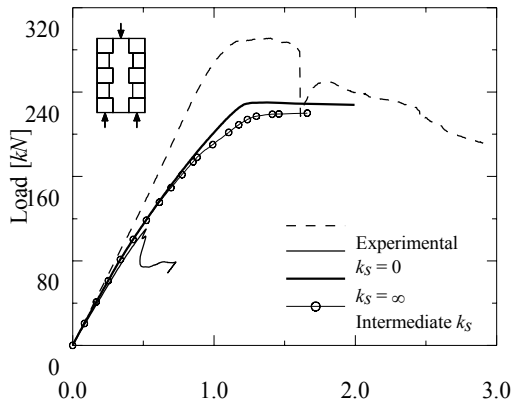

Figure 15. Numerical and experimental (NO2) load-displacement diagrams for keyed collar joints wallets. Different shear stiffnesses k_s were considered at the boundaries.

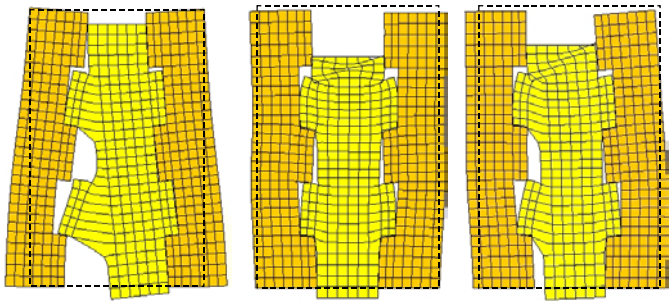

(a) (b) (c)

Figure 16. Deformed meshes at failure for different shear stiffnesses k_s at the supports: (a) $k_s = 0$, (b) $k_s = \infty$ and (c) int. k_s.

For the intermediate k_s at the supports, Figure 17 illustrates the contour of minimum principal stresses for the elastic regime and the principal plastic strains at failure. In Figure 17a, it is visible the transfer of compressive stresses from the inner-leaf to the outer-leaves, through the shear keys. In Figure 17b,c, the shearing-crushing of the inner-leaf near the top and the tensile damage in the inner-leaf, along the shear keys, is confirmed as failure mechanism.

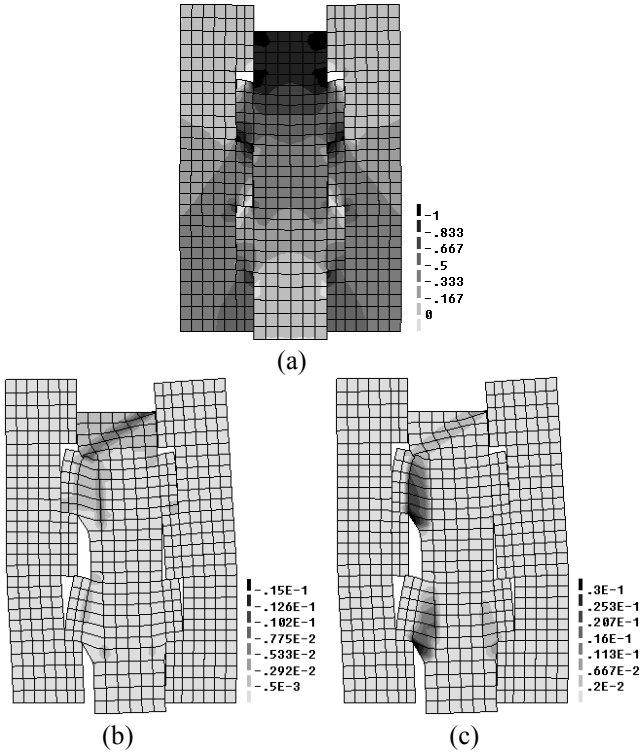

Figure 17. Results obtained for the shear simulations on keyed wallets, adopting the intermediate k_s: (a) principal minimum stresses for an applied load of 50 *kN* (elastic regime) and principal plastic strains at failure: (b) minimum and (c) maximum.

4.2 *Compression simulations on the full wallets*

The compression tests on wallets with and without shear keys have also been analysed. Friction between wallets and boundaries has been precluded in the simulations. In the case of the wallet with straight connections, a row of mesh elements at middle height was made slightly imperfect and a 10% lower compressive strength was given. The objective is to trigger the strain localization.

A comparison between numerical and experimental stress-strain diagrams is given in Figure 18. Good agreement is found in the case of the wallet with keyed collar joints. In the case of the wallet with straight collar joints, the predicted strength is about 20% higher than the experimental strength. As discussed in Section 3, the inner-leaf is almost not collaborating in the experimental response, which can partially explain the difference found between the experimental and numerical strength values.

Another point is that the numerical strength of the wallet with keyed connections is lower than the strength of the wallet with straight connections, as predicted also by the simple expressions discussed in Section 3. Such behaviour is explained by the smaller cross-sectional area of the outer-leaves in the case of the wallets with keyed collar joints.

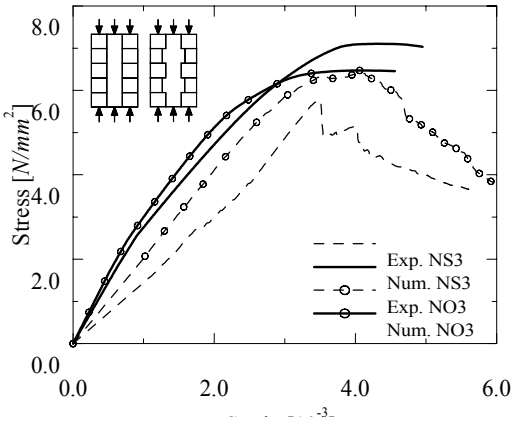

Figure 18. Stress-strain diagrams obtained for compression on wallets with straight collar joints (NS3) and keyed collar joints (NO3).

5 CONCLUSIONS

The present paper addresses the shear and compressive behaviour of composite masonry walls, which seems to be not a sufficiently debated issue in the literature. From the experimental tests, the following conclusions can be withdrawn:

a) Shear strength values found for straight collar joints are between 0.09-0.17 N/mm^2, whereas for keyed joints the values are in the 0.58-0.81 N/mm^2 range.
b) In wallets with straight collar joints, shear failure occurs due to vertical cracks that arise in the connections while in wallets with keyed collar joints, failure is mainly due to the development of diagonal cracks in the inner-leaf.
c) Further compression testing on composite wallets is needed, considering also specimens with different ratios between inner and outer-leaves thicknesses.

Numerical assessment of experimental data was also addressed. Good agreement has been found by utilizing a plasticity based finite-element model, in which units and mortar were smeared out in a continuum.

Simplified calculations for predicting the compressive strength of composite walls have also shown good agreement with experimental results and with advanced numerical methods. Thus, simplified expressions may be used as a first estimate of the wallets strength.

ACKNOWLEDGEMENTS

The experimental research was supported by MURST – Cof. 2000, 2002. Authors wish to thank M. Antico for technical assistance and M. Brazzale for data elaboration. FCT is gratefully acknowledged for the fellowship awarded to J. Pina-Henriques.

REFERENCES

Anzani, A., Binda, L., Fontana, A., Pina-Henriques, J. 2004. An experimental investigation on multiple-leaf stone masonry, in: *Proc. 13th IBMaC*, Amsterdam, the Netherlands.

Binda, L., Fontana, A., Anti, L. 1991. Load transfer in multiple leaf masonry walls, in: *Proc. 9th IBMaC*, Berlin, Germany.

Binda, L., Fontana, A., Mirabella G. 1994. Mechanical behaviour and stress distribution in multiple-leaf walls, in: *Proc. 10th IBMaC*, Calgary, Canada.

Binda, L., Saisi, A., De Benedictis, R., Tringali, S. 2003a. Exp. Study on the Damaged Pillars of the Noto Cathedral, in: *Proc. 8th Int. Conf. STREMAH*, Halkidiki, Greece.

Binda, L., Anzani, A., Pina-Henriques, J., Tongini Folli, R. 2003b. Sperimentazione su provini in muratura a tre paramenti, in: *Workshop: Danneggiamento, conserv. e manut. di strut. murarie e lignee*, DIS–Politecnico di Milano, Italy.

Binda, L., Anzani, A., Fontana, A. 2003c. Mechanical behaviour of multiple-leaf stone masonry: experimental research, in: *Int. Conf. Structural Faults & Repair*, London, UK.

CEN 1998. *Methods of test for masonry units: Det. of real and bulk density and of total and open porosity for natural stone masonry units*. EN 772-4, CEN, Brussels, Belgium.

CEN 1999. *Methods of test for mortar for masonry: Determination of flexural and compressive strength of hardened mortar*. EN 1015-11, CEN, Brussels, Belgium.

CEN 2000. *Methods of test for masonry units: Det. of compressive strength*. EN 772-1, CEN, Brussels, Belgium.

CEN 2002. *Methods of test for masonry: Determination of initial shear strength*. EN 1052-3, CEN, Brussels, Belgium.

Drei, A. and Fontana, A. 2001. Influence of geometrical and material properties on multiple-leaf walls behaviour, in: *Proc. 7th Int. Conf. STREMAH*, Bologna, Italy.

Egermann, R, Newald-Burg, C. 1994. Assessment of the load bearing capacity of historic multiple leaf masonry walls, in: *Proc. 10th IBMaC*, Calgary, Canada.

Lourenço, P. 1996a. *Computational strategies for masonry structures*. Dissertation, TU Delft, Delft, the Netherlands.

Lourenço, P. 1996b. *A user/programmer guide for the micro-modelling of masonry structures*. Report 03.21.1.31.35, TU Delft, Delft, the Netherlands.

Lourenço, P. 1997. *An anisotropic macro-model for masonry plates and shells: implementation and validation*. Report 03.21.1.31.07, TU Delft, Delft, the Netherlands.

Lourenço, P.B., Barros, J.O., Oliveira, J.T. 2004. Shear testing of stack bonded masonry. *Const. and Building Mat.*, 18.

Neville, A. 1997. *Prop. of concrete*. Wiley, New York, USA.

RILEM 1994. *Tension by splitting of concrete specimens*. CPC6, RILEM tech. rec., E&FN Spon, London, UK.
Van der Pluijm, R. 1999. *Out-of-plane bending of masonry, beh. and str*. Dissertation, TU Delft, Delft, the Netherlands.